Supporting information for

Unprecedented (4, 6)−connected net with mixed-valence $M_2^{II}M^{III}$ trinuclear and M_6^{II} hexanuclear clusters (M = Ni, Co): syntheses, crystal structures and magnetic properties

Lu Zhai,[a, b] Zhu−Xi Yang,[a] Wen−Wei Zhang,*[b] Jing−Lin Zuo,[b] Xiao−Ming Ren*[a,b,c]

[a] *State Key Laboratory of Materials−Oriented Chemical Engineering and College of Chemistry & Molecular Engineering, Nanjing Tech University, Nanjing 210009, P. R. China*

[b] *State Key Laboratory of Coordination Chemistry, School of Chemistry and Chemical Engineering, Nanjing University, Nanjing 210023 P. R. China*

[c] *College of Materials Science & Engineering, Nanjing Tech University, Nanjing 210009, P. R. China*

E−mail: wwzhang@nju.edu.cn (WWZ); xmren@njtech.edu.cn (XMR)

Table S1: Selected bond lengths (Å) and angles (^{o}) in **1** and **2**

For compound **1**

	Bond lengths (Å)		Bond angles (^{o})			
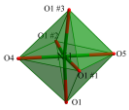	Ni1–O1	2.041(5)	O4–Ni1– O1	94.09(16)	O4–Ni1–O1#1	94.09(16)
	Ni1–O1#1	2.041(5)	O4–Ni1–O1#2	94.09(16)	O1–Ni1–O1#3	171.8(3)
	Ni1–O1#1	2.041(5)	O1#1–Ni1–O1#2	171.8(3)	O1#1–Ni1–O1	90.3(4)
	Ni1–O1#1	2.041(5)	O1–Ni1–O1#2	90.3(4)	O1–Ni1–O1#2	89.1(4)
	Ni1–O4	1.9851(19)	O1–Ni1–O1#3	89.1(4)	O4–Ni1–O5	180.0
	Ni1–O5	2.137(11)	O1#1–Ni1–O5	85.91(16)	O1–Ni1–O5	85.91(16)
	Bond lengths		Bond angles			
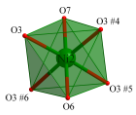	Ni2–O3	2.050(7)	O1#3–Ni2–O5	85.91(16)	O3–Ni2–O3#6	90.8(5)
	Ni2–O3#4	2.050(7)	O3#4–Ni2–O3#5	90.8(5)	O3–Ni2–O3#5	175.7(6)
	Ni2–O3#5	2.050(7)	O3#4–Ni2–O3#6	175.7(6)	O3#5–Ni2–O3#6	89.0(5)
	Ni2–O3#6	2.050(7)	O3–Ni2–O3#4	89.0(5)	O3–Ni2–O7	92.2(3)
	Ni2–O6	2.08(2)	O3#4–Ni2–O7	92.2(3)	O3–Ni2–O6	87.8(3)
	Ni2–O7	2.06(4)	O7–Ni2–O6	180.0(4)		
	Bond lengths		Bond angles			
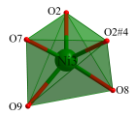	Ni3–O2	1.986(13)	O7–Ni3–O9	78.0(10)	O8–Ni3–O9	97.3(6)
	Ni3–O2#4	1.986(13)	O7–Ni3–O2	91.4(8)	O2–Ni3–O2#4	99.8(11)
	Ni3–O7	1.73(2)	O9–Ni3–O2	129.4(6)	O7–Ni3–O8	175.3(12)
	Ni3–O8	2.14(3)				
	Ni3–O9	1.963(6)				

Symmetry transformations used to generate equivalent atoms for **1**: #1=x, y, 1–z; #2=1–y, 1–x, z; #3=1–y, 1–x, 1–z; #4=y, x, z; #5=y, x, –z; #6=x, y, –z.

For compound **2**

	Bond lengths		Bond angles			
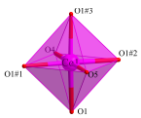	Co1–O1	2.079(5)	O6–Co1– O1	95.4(9)	O6–Co1–O1#1	95.4(9)
	Co1–O1#1	2.079(5)	O1–Co1–O1#1	102.8(12)	O5–Co1–O6	180.00(4)
	Co1–O1#2	2.079(5)	O1–Co1–O5	84.6(9)	O1#1–Co1–O5	84.6(9)
	Co1–O1#3	2.079(5)	O6–Co1–O2#2	91.4(9)	O1–Co1–O2#2	166.8(10)
	Co1–O4	2.0076(15)	O1–Co1–O2#3	87.8(4)	O1#1–Co1–O2#2	92.0(4)
	Co1–O5	2.152(11)	O1#1–Co1–O2#3	87.8(4)	O5–Co1–O2#2	88.6(9)
	Bond lengths		Bond angles			
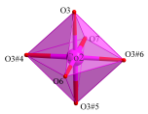	Co2–O3	2.063(7)	O4–Co2–O4#5	90.2(4)	O4–Co2–O4#4	89.7(4)
	Co2–O3#4	2.063(7)	O4#4–Co2–O4#5	177.8(5)	O4–Co2–O7	88.9(2)
	Co2–O3#5	2.063(7)	O4–Co2–O8	91.1(2)	O7–Co2–O8	180.00
	Co2–O3#6	2.063(7)				

	Co2–O6	2.10(2)				
	Co2–O7	2.07(3)				
	Bond lengths		Bond angles			
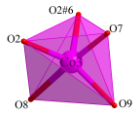	Co3–O2	2.076(13)	O8–Co3–O9	173.8(6)	O8–Co3–O3	89.6(4)
	Co3–O2#6	2.076(13)	O9–Co3–O3	94.3(3)	O8–Co3–O3#5	89.6(4)
	Co3–O7	1.828(19)	O9–Co3–O3#5	94.3(3)	O3–Co–O3#5	102.0(7)
	Co3–O8	2.18(2)				
	Co3–O9	2.024(5)				

Symmetry transformations used to generate equivalent atoms for **2**: #1=x, y, 1–z; #2=1–y, 1–x, z; #3=1–y, 1–x, 1–z; #4=x, y, –z; #5=y, x, –z, #6=y, x, z.

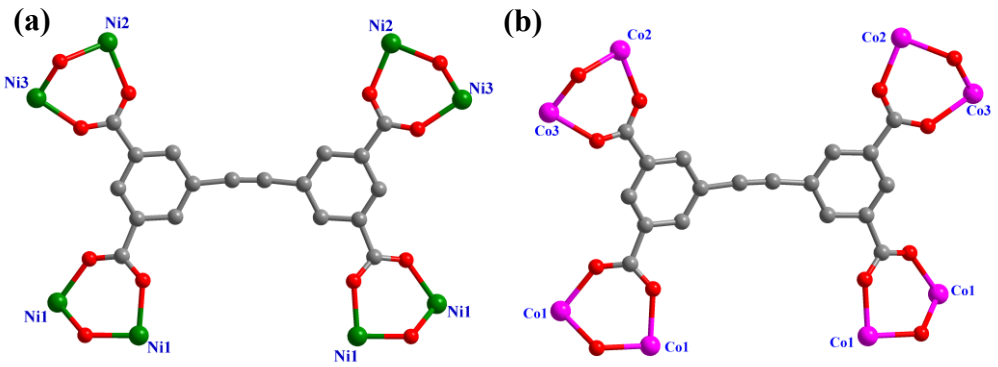

Figure S1. Coordination modes of the ligand in (a) **1** and (b) **2** and the two phenyl rings in $EBTC^{4-}$ ligand are almost coplanar (all hydrogen atoms were omitted for clarity) .

Bond valence sum (BVS) analysis

Bond valence sum (BVS) analysis was used to identify the central anion as hydroxo or oxo as well as the oxidation states of metal ions. The valence of a bond between two atoms, *i* and *j* is given by S_{ij}. The BVS for a given metal ion is the sum of bond valences for each bond made to that metal ion. The r_0 values are determined empirically such that the BVS is generally quite close to the oxidation state of the metal ion. In this work, *i* and *j* are Ni, O for compound **1** or Co, O for compound **2**. The charge *Vi* on one Ni1 or Co1 in the trinuclear M_3 unit is the sum of S_{ij} calculated from all six bonds connected to it, *ie*; the valence of the *i* atom. (See SI of *Chem. Commun.* **2007**, 840−842). B is a constant, the "universal parameter" ~0.37 Å. The

calculated results are shown in the following tables, which are closed to the literature result.

For **1**

Ni^{2+}	r_0	r_{ij}	B	$S_{ij}=\exp[(r_0-r_{ij})/B]$
Ni1–O1	1.670	2.042	0.370	0.366
Ni1–O1	1.670	2.042	0.370	0.366
Ni1–O1	1.670	2.042	0.370	0.366
Ni1–O1	1.670	2.042	0.370	0.366
Ni1–O4	1.670	1.986	0.370	0.426
Ni1–O5	1.670	2.138	0.370	0.282

$V_{Ni}=\Sigma S_{ij}=+2.172$; $V_{O4}=3\times S_{Ni1-O4}=1.278$

Ni^{3+}	r_0	r_{ij}	B	$S_{ij}=\exp[(r_0-r_{ij})/B]$
Ni1–O1	1.750	2.042	0.370	0.454
Ni1–O1	1.750	2.042	0.370	0.454
Ni1–O1	1.750	2.042	0.370	0.454
Ni1–O1	1.750	2.042	0.370	0.454
Ni1–O4	1.750	1.986	0.370	0.528
Ni1–O5	1.750	2.138	0.370	0.350

$V_{Ni}=\Sigma S_{ij}=+2.694$; $V_{O4}=3\times S_{Ni1-O4}=1.584$

For **2**

Values of r_0 for Co–O bonds for oxidation states +2 and +3 used in the analysis[1]

Co^{2+}	r_0	r_{ij}	B	$S_{ij}=\exp[(r_0-r_{ij})/B]$
Co1–O1	1.692	2.079	0.370	0.35136
Co1–O1	1.692	2.079	0.370	0.35136
Co1–O1	1.692	2.079	0.370	0.35136
Co1–O1	1.692	2.079	0.370	0.35136
Co1–O4	1.692	2.008	0.370	0.42615
Co1–O5	1.692	2.152	0.370	0.28845

$V_{Co}=\Sigma S_{ij}=+2.120$; $V_{O4}=3\times S_{Co1-O4}=1.278$

Co^{3+}	r_0	r_{ij}	B	$S_{ij}=\exp[(r_0-r_{ij})/B]$
Co1–O1	1.754	2.079	0.370	0.41546
Co1–O1	1.754	2.079	0.370	0.41546

Co1–O1	1.754	2.079	0.370	0.41546
Co1–O1	1.754	2.079	0.370	0.41546
Co1–O4	1.754	2.008	0.370	0.50334
Co1–O5	1.754	2.152	0.370	0.34107

$$V_{Co}=\Sigma S_{ij}=+\ 2.506; \quad V_{O4}=3\times S_{Co1-O4}=\ 1.510$$

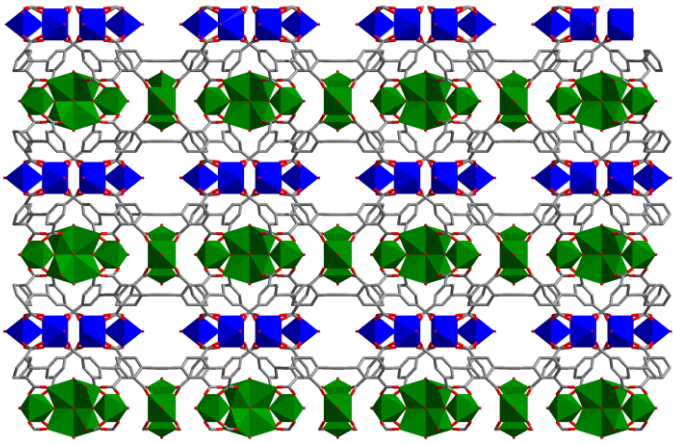

Figure S2. Polyhedral representation of the 3D framework of **1** showing layer structure along *b* axis (blue represents the trinuclear cluster and green represents the hexanuclear cluster in **1**, all hydrogen atoms are omitted for clarity).

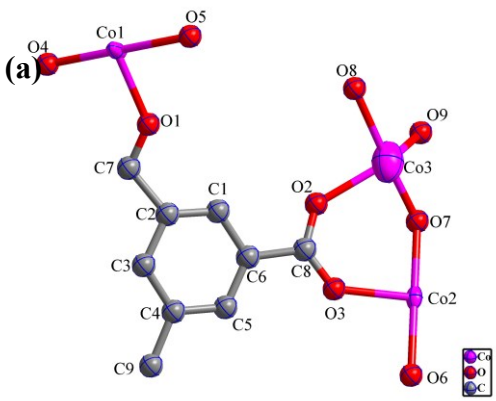

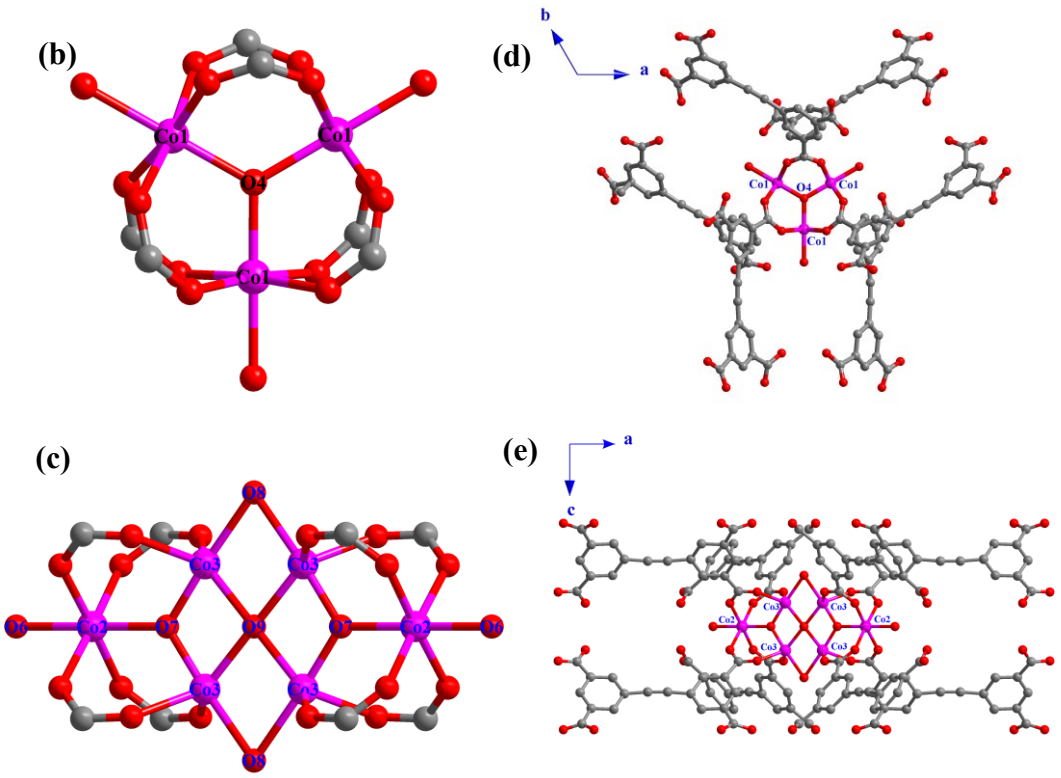

Figure S3. (a) An asymmetric unit of **2** with thermal ellipsoids at 50% probability level. (b) Perspective view of the trinuclear $[Co_3O(O_2C)_6]$ cluster and (c) the hexanuclear $[Co_6(\mu_3{-}O)_2(\mu_2{-}O)_2(O_2C)_8]$ cluster in **2**. (d) View of the trinuclear cluster and (e) the hexanuclear cluster as node being connected to six and eight $EBTC^{4-}$ ligands in **2**, respectively (all H atoms were omitted for clarity).

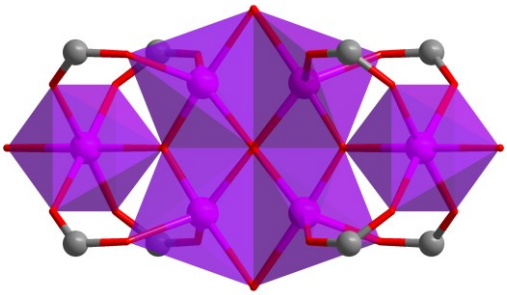

Figure S4. Polyhedral representation of the hexanuclear $\{Co_6O_{23}\}$ unit in **2**.

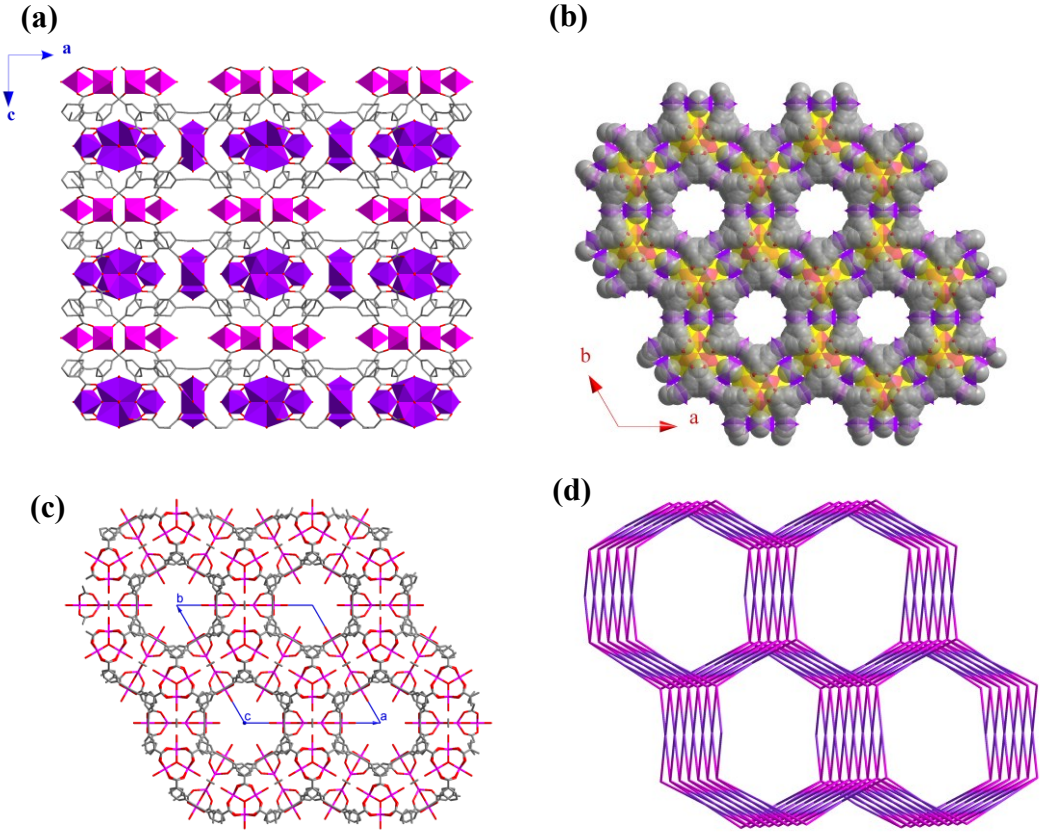

Figure S5. (a) Polyhedral representation of the 3D framework of **2** showing layer structure along the *b* axis. (b) The channels along the *c* axis surround by cages. (c) Representation of 3−D framework viewed along the *c* axis. (d) (4, 6)−connected network, where the pink represents the 6−connected node of trinuclear cluster and lavender represents the 4−connected node of the hexanuclear cluster in **2** (all H atoms were omitted for clarity).

The PXRD Patterns

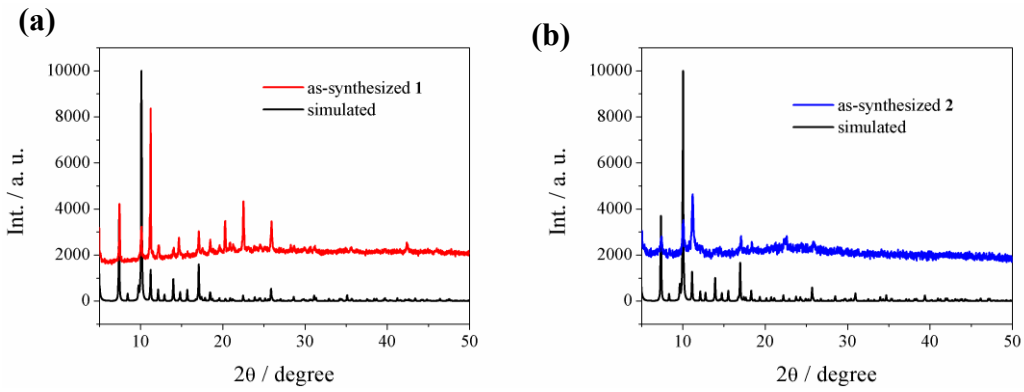

Figure S6. PXRD patterns of simulated from the X−ray single−crystal structures and

as–synthesized samples of **1** (a) and **2** (b) at ambient temperature.

The powder X–ray diffraction (PXRD) experiments for **1** and **2** were carried out carefully to check phase purity at room temperature. The patterns showed that the main peaks of the synthesized MOFs were closely consistent with those of the simulations from the single–crystal X–ray diffraction data, which imply high quality of the obtained products.

The IR Spectra

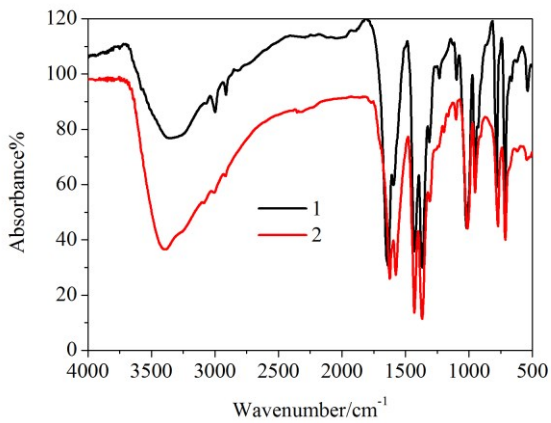

Figure S7. The IR spectra of **1** (black) and **2** (red) recorded from a KBr pellet.

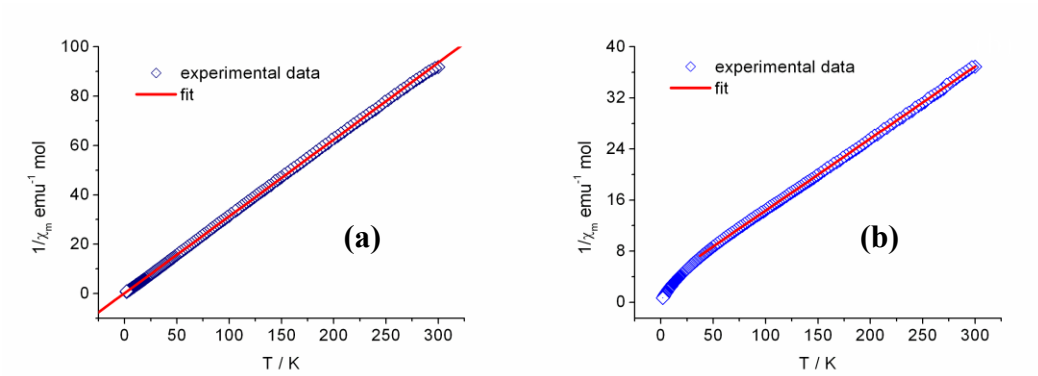

Figure S8. Reciprocal molar susceptibility as function of temperature for (a) **1** with C = 3.21 emu K mol^{-1}, θ = –0.59 K and R = 0.99993 and (b) **2** with C = 8.86 emu K mol^{-1}, θ = –27.35 K and R = 0.99995, where solid red line indicates Curie–Weiss fitting in the range 2–300 K.

References

1 Wood, R. M.; Palenik, G. J. *Inorg. Chem.* **1998**, 37, 4149–4151.